Zeitschrift für Kristallographie 212, 712–719

A neutron powder investigation of the high-temperature structure and phase transition in stoichiometric $LiNbO_3$

H. Lehnert*, H. Boysen, F. Frey

Universität München, Institut für Kristallographie und Angewandte Mineralogie, Theresienstr. 41, D-80333 München, Germany

A. Hewat and P. Radaelli

Institut Max von Laue – Paul Langevin, BP 156, F-38042 Grenoble Cedex 9, France

Received November 29, 1996; accepted January 20, 1997

Abstract. The structural changes of stoichiometric $LiNbO_3$ at temperatures up to 1470 K have been investigated by neutron powder diffraction. At $T_c \approx 1460$ K, $LiNbO_3$ transforms from a paraelectric high-temperature ($R\bar{3}c$) to a ferroelectric low temperature structure ($R3c$). The phase transition is of coupled order-disorder and displacive type. In the high-temperature phase, Li is highly disordered over two off-centre positions, whereas Nb takes a centrosymmetric position within O_6 octahedra. An analysis of anisotropic displacement parameters shows that the probability density function of Li is extended along c, that of the oxygens is more or less perpendicular to the Nb–O bonds, and that of Nb is slightly extended in the $a-b$ plane at high temperatures. An increase of the tilt angle of the NbO_6 octahedra away from an h.c.p. arrangement towards a perovskite structure was observed. The octahedra become almost regular at high temperatures. Comparison with an earlier investigation of congruent lithium niobate shows a quite similar behaviour, however, all parameters of the latter are closer to those of the perovskite structure at same temperatures.

Anomalies in the behaviour of the order parameters, a more complicated disorder and a high mobility of Li at high temperatures are explained by the competition of the order-disorder and displacive character of the phase transition.

1. Introduction

The outstanding physical properties (e.g. electro-optical, acousto-optical, electro-mechanical) of lithium niobate (LN), which have led to a wide range of technical applications, depend strongly on the exact composition. LN melts incongruently and most of the LN material is produced with the so-called congruent composition [Li]:[Nb] = 0.46 ($Li_{0.95}Nb_{1.01}O_3$), while strictly stoichiometric $LiNbO_3$ is more difficult to obtain. The high temperature structure and the phase transition from the low-temperature ferroelectric (space group $R3c$) to the high-temperature paraelectric phase ($R\bar{3}c$) of congruent LN have recently been studied by neutron powder diffraction by Boysen and Altdorfer (1994). Since these results may be influenced by defects in congruent LN (cation vacancies, excess Nb), a comparative study has been carried out on stoichiometric samples. Moreover, by using an extended data set ($\sin\theta/\lambda_{max} = 0.618$ Å^{-1}) as compared to that of Boysen and Altdorfer ($\sin\theta/\lambda_{max} = 0.544$ Å^{-1}) it was intended to put some of the previous conclusions, particularly the critical behaviour of the Debye-Waller factor on a more reliable basis.

The low-temperature phase of LN has been extensively studied previously by Abrahams, Reddy and Bernstein (1966), Abrahams, Hamilton and Reddy (1966), Abrahams, Levinstein and Reddy (1966) and Abrahams and Marsh (1986). The structure may be derived from a hexagonal close-packing of the oxygens with $^2/_3$ of the octahedral interstices filled with Nb and Li cations. Nb and Li are located on the three-fold axes, O atoms are in general position. The sequence along c is Nb–□–Li–Nb–... (□ = vacancy). Oxygen layers remain planar and equidistant, while the octahedra are slightly distorted and rotated. An alternate view of the LN structure, which has been put forward by Megaw (1968a), is a distorted perovskite structure, brought about mainly by a large (~ 20°) rotation of the NbO_6-octahedra around the three-fold axis. This view has been confirmed by Boysen and Altdorfer (1994) to be the more appropriate one in terms of crystal chemistry.

During the second-order phase transition into the high-temperature phase, Nb moves into the centrosymmetric site within its octahedron. For Li two models have been proposed in the literature: (I) in the displacive model, Li moves into a triangularly coordinated site within the oxygen layer below the former Li site, (II) in the order-disorder model, the Li atoms are randomly distributed on both sides of this oxygen plane. The disorder model was derived from a neutron scattering experiment on isostructural $LiTaO_3$ by Abrahams, Buehler, Hamilton and Laplace (1973).

* Correspondence author
(e-mail: harry@yoda.kri.physik.uni-muenchen.de)

The high temperature phase exists only in a narrow temperature range between T_c and the melting point T_m which is lower in stoichiometric ($T_c \approx 1460$ K, $T_m \approx 1500$ K) than in congruent LN ($T_c \approx 1430$ K, $T_m \approx 1530$ K). Basically, the disorder model was confirmed by Boysen and Altdorfer (1994), but there were also indications of a high mobility and a more complicated disorder behaviour of Li.

2. Experimental

The stoichiometric sample was kindly provided by Dr. Bauman of the University Paderborn. The stoichiometric composition was confirmed by the refined lattice constants at room temperature (see Table 1), which are close to the values given by Abrahams and Marsh (1986). The measurements were performed on the two-axis neutron powder-diffractometer D2B/ILL Grenoble with coarse primary collimation to obtain an optimum intensity at a wavelength of $\lambda = 1.5926$ Å. The angular range ($0° \leq 2\theta \leq 160°$ was scanned with 0.05° step width. The sample was kept in a Pt can (8 mm diameter, 10 mm height) and mounted in an ellipsoidal mirror furnace described by Lorenz et al. (1993). In this furnace it is possible to heat the sample in air to reduce Li_2O outdiffusion at high temperatures. By use of secondary collimators spurious scattering from the furnace (Al) could be suppressed, whereas Pt reflexions from the sample holder and the thermocouple (Pt–Pt/Rh 10%) appear in the diffraction pattern. These peaks suffered from extreme texture problems and had to be excluded from the fits. The temperature stability was about ±5 K and the absolute uncertainty including the gradient was about ±10 K. At 1490 K some recrystallization occurred and this data set was not considered further.

3. Data analysis and results

Analysis of the data was carried out using the Rietveld-program version of Thomas and Bendall (1978), extended for anharmonic Debye-Waller factors using a Gram-Charlier expansion up to fourth order (Boysen, 1992). Gaussian peak shapes and a manually defined background

Table 1. Final refined parameters: up to 1200 K model I, above 1200 K model II, 1470 K: high temperature phase. Atomic displacement parameters are given as U^O_{ij} [Å^2] where the superscript ^{O} refers to the OP coordinate system.

T [K]	a [Å]	c [Å]	R_{wp} [%]	GOF_{wp}	z (Li)	z (Nb)	x (O)
300	5.1444(1)	13.8495(2)	11.03	2.34	0.2996(5)	0.0199(2)	0.0478(3)
600	5.1720(1)	13.8670(2)	11.16	2.05	0.2960(5)	0.0200(2)	0.0503(3)
900	5.2039(1)	13.8780(2)	10.30	1.70	0.2924(8)	0.0184(2)	0.0529(4)
1200	5.2397(1)	13.8744(2)	9.43	1.38	0.2921(9)	0.0155(2)	0.0560(5)
1250	5.2459(1)	13.8711(3)	12.38	1.77	0.287(1)	0.0148(3)	0.0579(6)
1300	5.2528(1)	13.8676(3)	12.48	1.75	0.289(1)	0.0137(3)	0.0581(6)
1350	5.2598(2)	13.8624(3)	13.41	1.79	0.289(1)	0.0117(3)	0.0585(8)
1400	5.2660(2)	13.8577(4)	15.43	1.96	0.287(1)	0.0109(4)	0.0592(9)
1425	5.2680(2)	13.8556(4)	14.95	1.86	0.287(1)	0.0106(4)	0.0601(9)
1450	5.2700(3)	13.8530(5)	18.44	2.28	0.283(1)	0.0103(6)	0.0615(9)
1470	5,2727(3)	13.8509(6)	18.64	2.20	0.286(1)	0	0.0576(4)

T [K]	y (O)	n (Li)	U^O_{11} (Li)	U^O_{33} (Li)	U^O_{11} (Nb)	U^O_{33} (Nb)
300	0.3439(4)	0.97(3)	0.14(5)	0.45(9)	0.081(9)	0.036(12)
600	0.3416(5)	0.91(2)	0.45(6)	0.32(11)	0.154(10)	0.117(13)
900	0.3398(5)	0.91(2)	0.49(6)	1.53(23)	0.272(10)	0.220(13)
1200	0.3409(7)	0.85(2)	0.54(7)	1.78(30)	0.416(9)	0.335(15)
1250	0.3393(9)	0.64(5)/0.17(5)	0.52(9)	0.89(28)	0.431(13)	0.346(19)
1300	0.3387(1)	0.75(6)/0.13(6)	0.69(10)	1.21(32)	0.449(13)	0.333(19)
1350	0.3382(13)	0.81(8)/0.10(6)	0.78(10)	1.51(37)	0.476(14)	0.336(19)
1400	0.3378(17)	0.71(10)/0.17(10)	0.84(14)	1.52(45)	0.557(18)	0.407(25)
1425	0.3396(16)	0.72(11)/0.13(9)	0.90(14)	1.63(4(9	0.573(18)	0.419(25)
1450	0.3421(12)	0.78(12)/0.02(10)	0.80(17)	0.90(46)	0.600(23)	0.340(27)
1470	$^1/_3$	0.91(5)	0.99(18)	1.73(41)	0.643(23)	0.391(31)

T [K]	U^O_{11} (O)	U^O_{22} (O)	U^O_{33} (O)	U^O_{12} (O)	U^O_{13} (O)	U^O_{23} (O)
300	0.128(14)	0.097(22)	0.146(8)	−0.028(22)	−0.021(14)	−0.018(15)
600	0.302(16)	0.200(25)	0.250(10)	−0.003(27)	−0.043(16)	−0.037(16)
900	0.447(17)	0.368(28)	0.381(10)	−0.036(30)	−0.135(14)	−0.030(16)
1200	0.585(20)	0.471(30)	0.508(10)	−0.068(35)	−0.122(16)	−0.094/16)
1250	0.602(28)	0.489(40)	0.583(13)	−0.058(48)	−0.069(23)	−0.170(23)
1300	0.605(32)	0.537(48)	0.592(15)	−0.060(58)	−0.122(25)	−0.130(24)
1350	0.708(39)	0.540(57)	0.628(15)	−0.034(70)	−0.152(30)	−0.138(27)
1400	0.666(47)	0.652(68)	0.647(19)	−0.114(84)	−0.056(37)	−0.260(33)
1425	0.768(44)	0.640(65)	0.607(17)	−0.073(79)	−0.034(37)	−0.247(32)
1450	0.556(43)	0.812(70)	0.683(23)	−0.134(79)	−0.053(42)	−0.214(37)
1470	0.696(18)	0.560(29)	0.689(30)	−0.118(21)	−0.139(9)	−0.160(23)

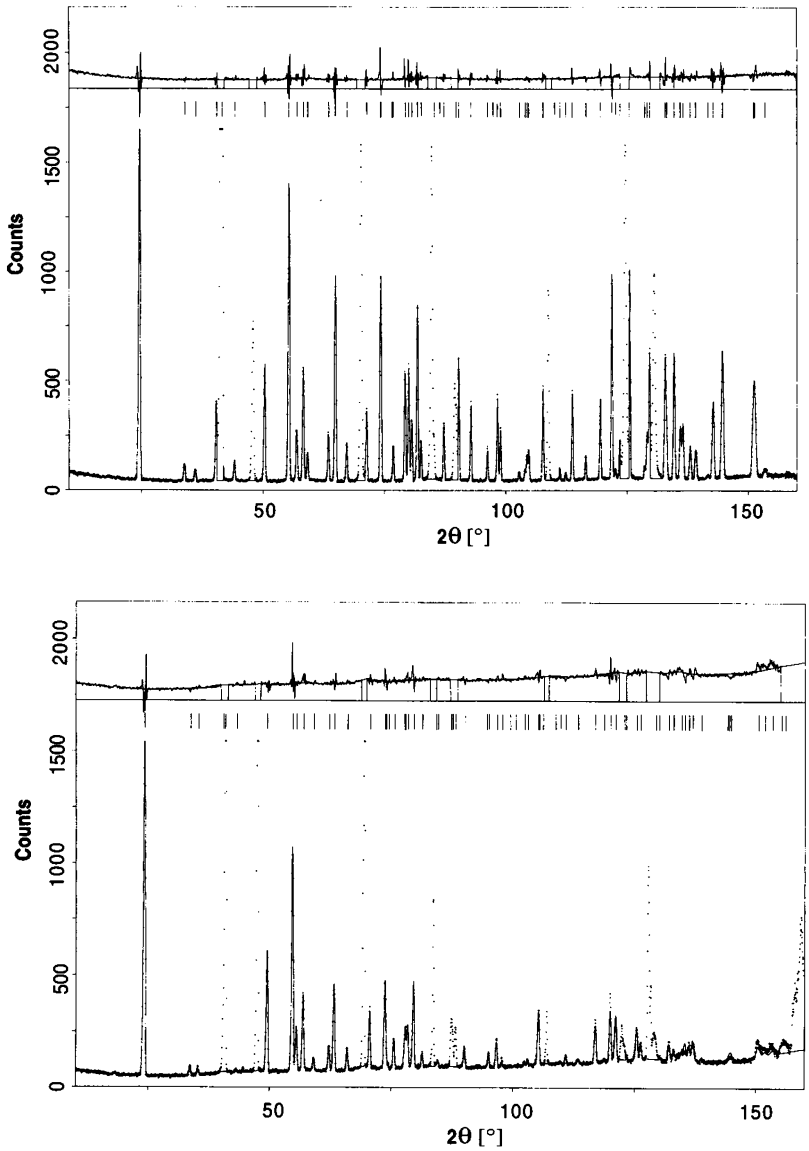

Fig. 1. Observed (dots) and calculated (solid line) powder patterns at 300 K (**a**) and 1250 K (**b**). The background ($y_{obs} - y_{calc}$) is shown at the top. Reflexions positions are marked, Pt reflexions are excluded from the fit.

were used. Neutron scattering lengths were taken from the compilation of Koester, Rauch and Seymann (Sears, 1992): $b_{Li} = -1.90(2)$ fm, $b_{Nb} = 7.054(3)$ fm and $b_O = 5.803(4)$ fm. Examples of observed and calculated powder patterns are shown in Fig. 1.

Basically two models have been tried:

Model I, with 3 atoms in the asymmetric unit, corresponding to a purely displacive transition:

Li	0	0	z,	$z_{Li} = {}^1/_4 + \Delta z_{Li}$
Nb	0	0	z,	$z_{Nb} = \Delta z_{Nb}$
O	x	y	z,	$y_O = {}^1/_3 + \Delta y_O$, $z_O = {}^1/_{12}$

(fixed in the polar space group),

Model II, with 4 atoms corresponding to an order-disorder transition. An additional Li′ atom is placed in the "empty" octahedron:

Li′	0	0	z,	$z_{Li'} = {}^1/_4 - \Delta z_{Li'}$.

In the high temperature phase, Δz_{Nb} and Δy_O become zero. In the displacive model $\Delta z_{Li} = 0$, whereas in the order-disorder model both Li sites become related by an inversion centre $\Delta z_{Li} = -\Delta z_{Li'}$ and the occupancy becomes ${}^1/_2$. In principle z_{Li} and $z_{Li'}$ are independent below T_c, however, because of problems during the fits, we constrained $z_{Li} + z_{Li'} = {}^1/_2$ and the corresponding atomic displacement parameters (ADP's). Below 1200 K no evidence for an occupation of the Li′ site was found, and results are given in Table 1 for model I only. Above 1200 K model II yielded only slightly better agreement factors, which by itself is not very significant. However, the refined parameters (especially the ADP's, and the total Li occupancies) are much more reasonable. Therefore these results are included in Table 1.

A problem occurred for the 1450 K data set. Two different models gave an almost identical R-factor (with clear minima on the hyperplane in parameter space): one with Li preferentially in its regular octahedron and one with Li in the vacant octahedron (i.e. in the Li′ position). In the latter case Δz_{Nb} is considerably smaller, which might seem to be more reasonable with respect to the temperature behaviour of this parameter (see below). A similar type of reversal was found for congruent LN (see Boysen and Altdorfer). The hypothesis that the sample was in the high

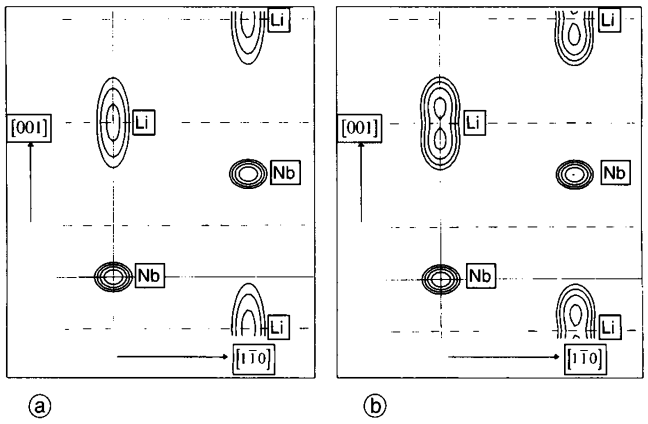

Fig. 2. P.d.f. maps of Li and Nb at 1200 K, (1$\bar{1}$0)-section, of the displacive model (**a**) and of the order-disorder-model (**b**). Dashed lines indicates the position of the oxygen layers.

temperature phase at this temperature could be clearly rejected on the basis of the *R*-factors. Only at 1470 K the space group $R\bar{3}c$ applies. The fit is slightly better for the order-disorder model, but only moderately significant. In fact, the two models may be considered to be not too different. This is illustrated in Fig. 2. The Li density is considerably smeared out in the *c*-direction to almost the same extent and there are only faint maxima in the order-disorder model. Both models indicate strong (probably dynamic, see below) disorder. In other words, the distinction between a displacive and an order-disorder transition, which has been discussed controversially in the literature for a long time, may in fact be meaningless: for a heavily disordered atom the definition of its position looses its sense.

As may be seen from Table 1, the total occupancies of Li at temperatures above RT are generally too low, which indicates further disorder. A number of refinements were therefore carried out using additional split positions (also for Nb and O) as well as anharmonic Debye-Waller factors. Some gave slightly better GOF's and higher total occupancies of Li, in agreement with the values expected for a stoichiometric compound. However, the reduction of the *R*-factors was not significant at all temperatures, some ADP's were not physically meaningful and had large errors. Also difference Fourier analyses were not successful. Similar problems have been reported by Boysen and Altdorfer (1994), who assigned them to the poor overdetermination, which is much better in the present case (123–126 reflexion, 12–17 structural parameters). A hint for some systematic errors is evident from Fig. 3. The GOF decreases with temperature up to about 1200 K (which is expected according to the decrease of the total intensity due to the Debye-Waller factor), while above this temperature it increases strongly again. A possible explanation is as follows. In single crystals of LN partial domain reversal of the ferroelectric domains (polarity) occurs close to T_c (e.g. Nakamura, Ando and Shimizu, 1987), the reasons still being a subject of discussion in the literature (thermal gradients, strains, outdiffusion of Li_2O). It is therefore conceivable that domain inversion may also take place within the grains of the powder sample. If these domains, including the walls in between, are smaller than the coherence length of the neutrons, the kinematic theory of diffraction fails. A further support for this explanation comes from the fact that the peaks broaden slightly with increasing temperature, although a simple analysis in terms of particle size and strains was not successful. This situation is not covered by any available Rietveld program.

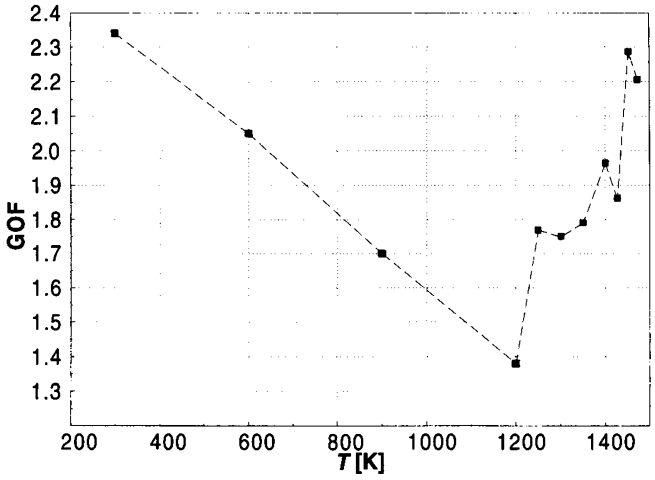

Fig. 3. Temperature dependence of the $GOF_{wp} = R_{wp}/R_{p\,exp} = [\sum w(y_{obs} - y_{calc})^2/(m-p)]^{1/2}$, [$y$ are the individual profile intensities, w their weights, m the number of data points and p the total (= structural + instrumental) number of refinable parameters].

4. Discussion

A detailed symmetry analysis of the phase transition was given by Boysen and Altdorfer (1994). There are essentially four critical order parameter transforming as the irreducible representation (IR) $A_{2u}(\Gamma^{2-})$: φ_1 (connected with $\Delta z_{Li} + \Delta z_{Li'}$), φ_2 (Δz_{Nb}), φ_3 ($\Delta x_O + 2\Delta x_O$), η $[(n_{Li} - n_{Li'})/(n_{Li} + n_{Li'})]$ and two non-critical (A_{1g}, Γ^{1+}) ones: φ_5 ($\Delta z_{Li} - \Delta z_{Li'}$), and φ_6 (Δx_O).

Fig. 4 shows the temperature dependence of the order parameters Q_i corresponding to the critical modes, normalised at 300 K [$Q_i = \varphi_i(T)/\varphi_i$ (300 K)]. φ_2 shows an expected critical behaviour for a second order phase transi-

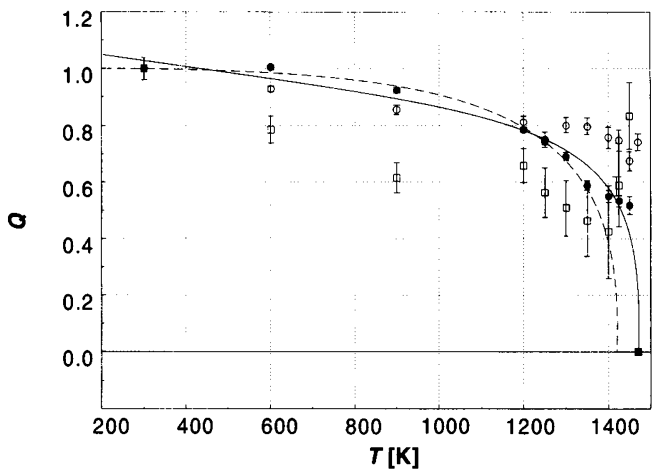

Fig. 4. Temperature dependence of normalised order parameters: Q_1(○), Q_2 (●), Q_3 (□) [$Q_i = \varphi_i(T)/\varphi_i$(300 K)]. Lines represent fits of a critical law to Q_2 only for all temperature points (solid line) and up to 1350 K (dashed line).

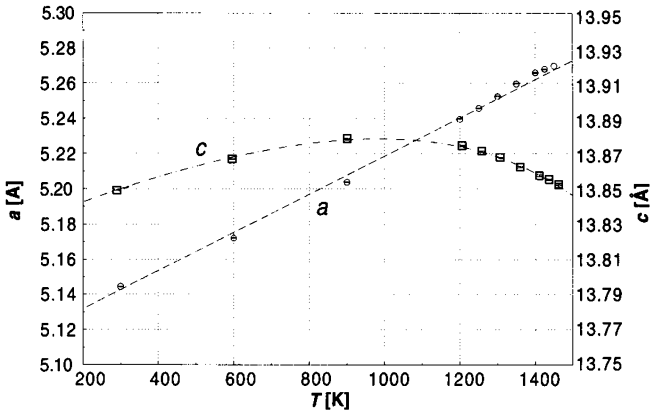

Fig. 5. Temperature dependence of the lattice parameter: a (○), c (□). Error bars are smaller than the symbols.

tion (the movement of Nb is considered as the primary order parameter), but only up to 1350 K, above which the decrease is much slower suggesting even a first order behaviour in the final stages. It should be emphasised, that these deviations are not caused by large temperature uncertainties, as evidenced by the continuous behaviour of the lattice constants (Fig. 5). A fit to the critical law $Q_2 = [(T_c - T)/T_c]^{\beta}$ for all data points gave $T_c =$ 1467(29) K and $\beta = 0.20(6)$ which is the solid curve in Fig. 4. Using only data points up to 1350 K (broken curve in Fig. 4) yielded $T_c = 1424(72)$ K and $\beta = 0.27(2)°$. Clearly T_c is too low in this case which therefore assigns some reality to the behaviour above 1350 K (see below). Q_3 lies below this curve with an abrupt decrease at 1400 K, however, with large errors. To calculate Q_1 for the disorder model, z_{Li} and $z_{Li'}$ are needed separately which were, however, not available (see above). Therefore Q_1 is plotted for the displacive model. After an initial decrease, this parameter stays far above $^1/_4$ and approaches the non-zero value of model II in the high temperature phase. Not included in Fig. 4 is the variation of η, the genuine order-disorder order parameter. As may bee seen from the occupancies n given in Table 1 this parameter shows only little variation with temperature, i.e. there are no precursor effects as should be expected for simple second order order-disorder transition. From Landau theory in the lowest order, all order parameters belonging to the same irreducible representation should show the same temperature behaviour. This is clearly not the case. A similar result was found for the phase transition in $NiTiO_3$ (Boysen, Frey, Lerch and Vogt, 1995) where this was assigned to the coupling to non-critical order parameters leading to higher order terms in the Landau expansion. Another explanation could be the existence of two competing order parameters. This will be discussed below.

A critical behaviour of the Debye-Waller factor is expected for those components which lie along the directions of the order parameter (see Boysen and Lerch, 1996, for a derivation in the frame of the Landau theory). The temperature dependence of the ADP's U_{ij} of the cations are shown in Fig. 6 and Fig. 7. No anomaly is expected for U_{11}(Li) and U_{11}(Nb), since there is no order parameter corresponding to this direction. For Li this is approximately true, while there is a non-linear increase for

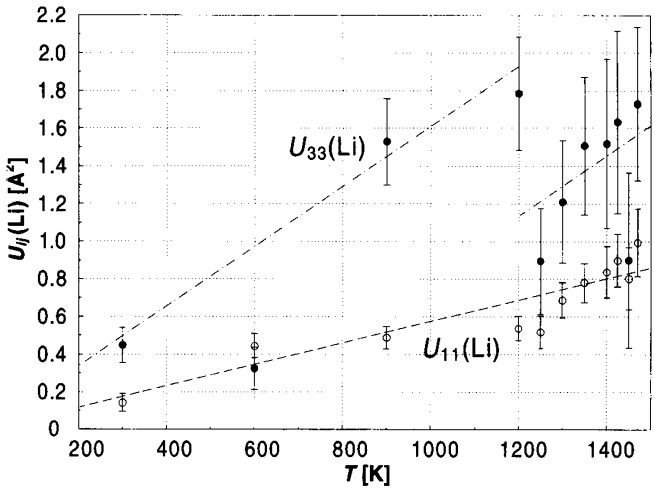

Fig. 6. Temperature dependence of the atomic displacement parameters, U_{11}(Li) (○), U_{33}(Li) (●).

U_{11}(Nb). U_{33}(Li) and U_{33}(Nb) correspond to φ_1 and φ_2, respectively. The abrupt change of U_{33}(Li) at 1200 K is probably related to the change of the model (see above) and cannot be taken as a real anomaly. Unfortunately, the errors are too large to draw any definitive conclusions about the critical behaviour. The temperature variation of the U_{ij} of the oxygen, as refined, i.e. corresponding to the crystal axes system, shows no anomalies. Nevertheless, in order to relate them to the different order parameters, the coordinate system has to be transformed according to their directions. This order parameters system is defined by φ_6 ([100]), φ_3 ([120]) and φ_1 (or φ_2, etc.) ([001]), see Boysen and Altdorfer (1994). A remarkable result of this procedure is that $U^O{}_{12}$ is almost zero in the order parameter system, in contrast to U_{12} in the crystal system as shown in Fig. 8 (U_{13} and U_{23} are small in both cases), which means that the thermal ellipsoid has indeed its main axes parallel to the directions of the OP. Unfortunately, however, the errors are again too large to be conclusive and therefore the results for the oxygen have been omitted for brevity.

In the theoretical analysis of the $LiNbO_3$ structure given by Megaw (1968a, b; see also Megaw, 1973; Megaw

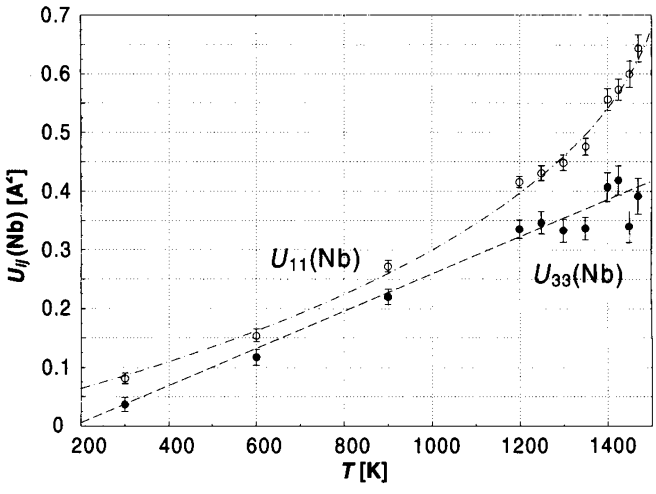

Fig. 7. Temperature dependence of U_{11}(Nb) (○), U_{33}(Nb) (●).

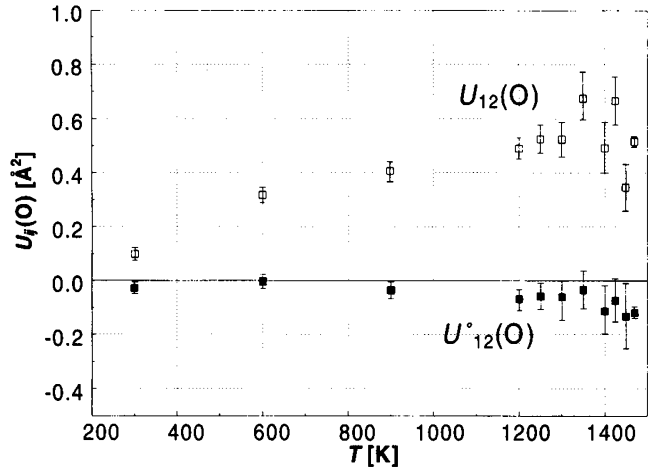

Fig. 8. Temperature dependence of U_{12} (O) (□), corresponding to the crystal axes system, and U^{O}_{12} (○) (■), transformed to the order parameter coordinate system.

and Darlington, 1975), the structure is envisaged as a corner-linked framework of NbO_6 octahedra, thereby emphasising the much stronger Nb–O bonds as compared to the Li–O bonds. In agreement with this picture the thermal ellipsoids of O are found to be basically perpendicular to the Nb–O-bonds, thus indicating rotational motions of these octahedra.

By rotating the NbO_6 octahedron around the threefold axis it is possible to go continuously from the h.c.p. structure to the perovskite structure. This tilt angle ω, which is related to φ_6, is given by

$$\tan \omega = 3(3)^{1/2}\, u/(2 - 3u)$$

where $u = \Delta x_O = 0$ ($\omega = 0°$) corresponds to ideal close packing and $u = {}^1/_6$ ($\omega = 30°$) to ideal perovskite. The temperature behaviour is shown in Fig. 9. There is no anomaly at T_c as expected for this non-critical parameter and its increase with temperature indicates a tendency towards the perovskite structure as anticipated by Megaw and confirmed for congruent LN by Boysen and Altdorfer (1994). Similary the octahedron strain ζ, as defined by Megaw and Darlington (1975), which describes a flattening or elongation of the octahedra

$$c/a = \{2(6)^{1/2}/[\sin \omega + (3)^{1/2} \cos \omega]\}\,(1 + \zeta)$$

decreases with temperature (Fig. 9), i.e. the octahedra become more regular, as is the case in the perovskite structure.

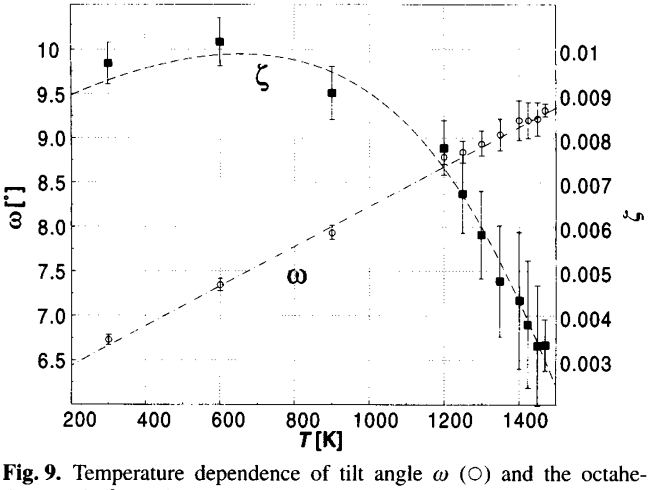

Fig. 9. Temperature dependence of tilt angle ω (○) and the octahedron strain ζ (■) in the NbO_6-Octahedra.

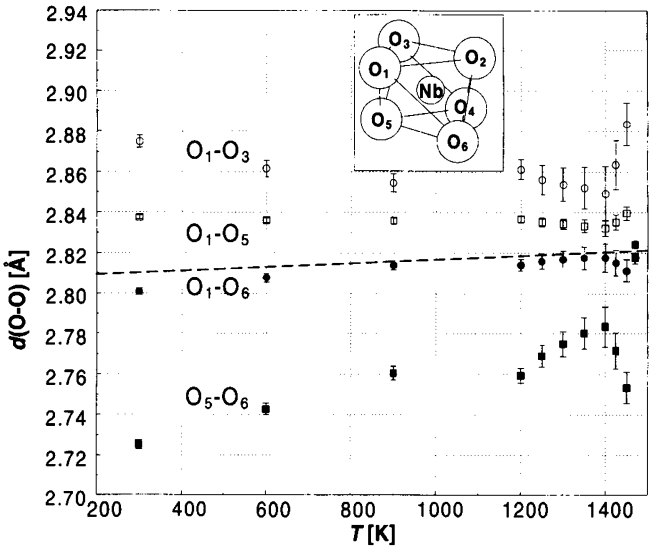

Fig. 10. Temperature dependence of O–O bond lengths in NbO_6. octahedron: O_1–O_3 (○), O_5–O_6 (■), O_1–O_5 (□), O_1–O_6 (●), see inset for numbering the atoms. The average bond length is shown by the dashed line.

Fig. 10 shows the temperature dependence of the O–O bond lengths in the NbO_6 octahedron. The increasing regularity holds up to 1400 K, then the oxygen triangle above Nb opens up again. This happens together with the retardation of the movement of Nb into the centrosymmetric position. On the other hand, the Nb–O distance (Fig. 12) follows a smooth critical behaviour. This is in contrast with congruent LN, where Boysen and Altdorfer (1994) found a linear change up to T_c and a rather abrupt jump near T_c. The average distance between Nb and O remains almost constant. The Nb–O–Nb bond angle increases from 138° at RT to about 147° at T_c, i.e. there is also a tendency towards the "perovskite value" of 180°.

The tilting of the octahedron is accompanied by an opening of the oxygen triangle between the Li and the □-octahedron. This is shown by the radius r, the distance between oxygen and the centre of the oxygen triangle in Fig. 11. Indicated by the horizontal line in Fig. 11 is the Li–O distance at low temperatures, which can be taken as the equilibrium bond length between these two atoms. This picture suggests a very simple explanation of the phase transition. It takes place as soon as the opening of the oxygen triangle is wide enough that Li can pass through this "bottle neck". At higher temperatures the opening becomes even too large to "bond" Li at its centre. As a consequence Li becomes mobile, diffusing around this position. The transition itself may thus also be termed as one to a "super-ionic-conduction state". Note that the "break even" point (the crossing of the two lines in Fig. 11) is below T_c, roughly at a temperature where φ_2 (Δz_{Nb}) starts to deviate from its smooth "second order" behaviour (Fig. 4). Consequently the phase transition may

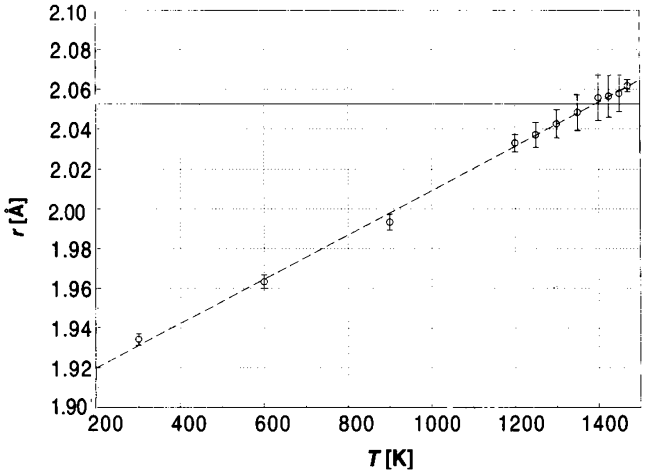

Fig. 11. Temperature dependence of the opening of the O-triangle between the Li- and □-octahedron indicated by r, the distance between oxygen and the centre of the oxygen triangle. The solid line indicates the Li–O bond length at RT.

be described by the competition of two different ordering mechanisms: a "superionic" and a "ferroelectric" one.

Though appealing, this view of the transition mechanism may be questioned with regard to the relatively large esd's shown in Fig. 11. There are, however, further arguments to support this. The non-proportionality between the different OP's belonging to the same IR is typical for two competing OP's with different T_c's. In particular, η describing the order-disorder process of Li shows a behaviour more like a first order transition. Though by itself belonging to the critical IR A_{2u} it is initiated by the action of non-critical parameter φ_6 (Δx_O), belonging to A_{1g}, the opening of the oxygen triangle discussed above. The initially smooth behaviour of the displacive degree of freedom aiming at a transition temperature $T_c' < T_c$ (compared to the fit of Q_2, dashed curve in Fig. 4) is interrupted by the onset of the Li disordering with transition temperature at T_c. Li entering the □-octahedron leads to a reopening of the oxygen-triangle above Nb (O_1–O_2–O_3 in Fig. 10) which in turn leads to a slower decrease of z_{Nb} in the region $T_c' < T < T_c$, such that the Nb–O distance (Fig. 12) retain their smooth variation with temperature. Li

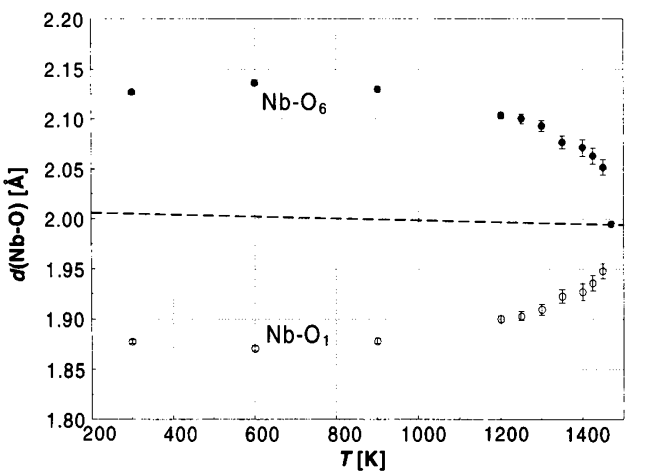

Fig. 12. Temperature dependence of Nb–O bond lengths (○, ●), Dash-dotted line indicates the average of the Nb–O bond lengths.

enters the □-octahedron not directly to the Li′ site, assumed for a pure order-disorder transition (model II), but stays close to the oxygen plane. This is exemplified in Fig. 13, which shows the probability density function (p.d.f.) of Li (and Nb) at 1400 K, derived from anharmonic refinement and Fourier transformation of Debye-Waller factors. The Li density is considerably spread out, extending partly into the □-octahedron and showing a three-fold anisotropy around the triad. The refinement of the anharmonic model did not result in a significantly lower GOF as compared to the split model (Table 1). It may, however, easily be understood that neither model gives a good representation of the "true" pdf of Li. The anharmonic model is limited by the Gram-Charlier series expansion and the split model had to be constrained to equal distances from the oxygen plane. The available data did not allow to refine more sophisticated models (higher order terms in the expansion, additional split atoms). These limitations may also explain the increase of the GOF's above 1200 K (Fig. 3). In any case, the heavy disorder of Li makes an unambiguous definition of the order-disorder OP impossible.

The pdf in Fig. 13 shows further lobes in [2$\bar{2}$1] direction which corresponds to the chain disorder derived from the diffuse scattering in congruent LN (Zotov, Frey, Boysen, Lehnert, Hornsteiner, Strauß, Sonntag, Mayer, Güthoff and Hohlwein, 1995). This may be an indication that stoichiometric LN is also not well ordered but includes some kind of defect structure in agreement with recent findings of Lehnert, Boysen and Ouladdiaf (to be published) that stoichiometric single crystals of LN show similar diffuse scattering as congruent ones. Finally, it has been already recognised by Zotov et al. (1995), on the basis of the room temperature observations of Iyi, Kitamura, Izumi, Yamamoto, Hayashi, Asano and Kimura (1992) in LN with different composition and the temperature dependent results of Boysen and Altdorfer (1994) on congruent LN that there is a general tendency towards the perovskite structure with increasing static (number of de-

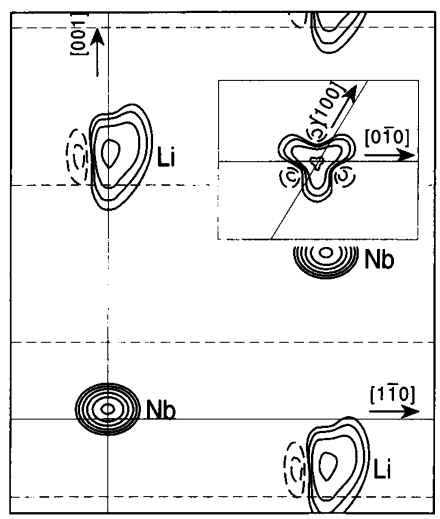

Fig. 13. P.d.f. maps of Li (and Nb) at 1400 K (1$\bar{1}$0)-section. Small dashed lines indicate negative regions. Long dashed lines (straight) show the positions of the oxygen layers. The inset shows a (001)-section through the Li position.

fects) and dynamic (temperature) disorder. This is confirmed by the present study: all parameters of congruent LN are closer to their values in perovskite than those of stoichiometric LN at same temperatures. An alternate view is that the congruent LN is closer to the transition temperature which is about 100 K lower than in stoichiometric LN.

5. Conclusion

It was found that only the movement of Nb shows the expected critical behaviour for a second order phase transition, until close to T_c the decrease is retarded suggesting even a first order behaviour in the final stages. The other order parameters belonging to the same irreducible representation do not show the same temperature behaviour in contrast to the expectation. U_{11}(Nb) increases non-linearly with temperature, although there is no order parameter corresponding to this direction. The temperature variation of the U_{ij} of oxygen shows no anomalies. $U^0{}_{12}$ is almost zero in the order parameter system, in contrast to U_{12} in the crystal system, which means that the thermal ellipsoid has indeed its main axes parallel to the directions of the OP. The NbO_6 octahedra become more regular and the tilt angle ω increases with temperature indicating a tendency away from the h.c.p. structure towards the perovskite structure. The tilting of the octahedron is accompanied by an opening of the oxygen triangle between the Li and the □-octahedron wide enough that Li can pass through and become mobile, diffusing around the centre of the oxygen triangle. This happens below T_c, roughly at a temperature where $\varphi_2(\Delta z_{Nb})$ starts to deviate from its smooth "second order" behaviour. Therefore the phase transition may be described by the competition of two different ordering mechanisms: a "superionic" and a "ferroelectric" one. In comparison with congruent LN, all parameters of congruent LN are closer to their values in perovskite than those of stoichiometric LN at the same temperatures.

Acknowledgments. We are grateful to Dr. I. Bauman (University of Paderborn) for supplying the sample. The work was supported by funds of the DFG under Fr747/6-1.

References

Abrahams, S. C.; Buehler, E.; Hamilton, W. C.; Laplaca, S. J.: Ferroelectric lithium tantalate-III. Temperature dependence of the structure in the ferroelectric phase and the paraelectric phase at 940 °K. J. Phys. Chem. Solids **34** (1973) 521–532.

Abrahams, S. C.; Hamilton, W. C.; Reddy, J. M.: Ferroelectric lithium niobate. 4. Single crystal neutron diffraction study at 24 °C. J. Phys. Chem. Solids **27** (1966) 1013–1018.

Abrahams, S. C.; Levinstein, H. J.; Reddy, J. M.: Ferroelectric lithium niobate. 5. Polycrystal X-ray diffraction study between 24° and 1200 °C. J. Phys. Chem. Solids **27** (1966) 1019–1026.

Abrahams, S. C.; Marsh, P.: Defect structure dependence on composition in lithium niobate. Acta Crystallogr. B**42** (1986) 61–68.

Abrahams, S. C.; Reddy, J. M.; Bernstein, J. L.: Ferroelectric Lithium Niobate. 3. Single crystal X-ray diffraction study at 24 °C. J. Phys. Chem. Solids **27** (1966) 997–1012.

Boysen, H.: Anharmonic thermal parameters, disorder and phase transition, In: *Accuracy in Powder Diffraction II.* (Eds. E. Prince, J. K. Stalick), p. 165–174. NIST Special Publication 846, Washington 1992.

Boysen, H.; Altdorfer, F.: A neutron powder investigation of the high-temperature structure and phase transition in $LiNbO_3$. Acta Crystallogr. B**50** (1994) 405–414.

Boysen, H.; Frey, F.; Lerch, M.; Vogt, Th.: A neutron powder investigation of the high-temperature phase transition in $NiTiO_3$. Z. Kristallogr. **210** (1995) 328–337.

Boysen, H.; Lerch, M.: Order parameter coupling and Debye-Waller factor at the phase transition in $NiTiO_3$. Phase Transitions **59** (1996) 1–24.

Iyi, N.; Kitamura, K.; Izumi, F.; Yamamoto, J. K.; Hayashi, T..; Asano, H.; Kimura, S.: Comparative study of defect structures in lithium niobate with different composition. Solid State Chem. **101** (1992) 340.

Lorenz, G.; Neder, R.; Marxreiter, J.; Frey, F.; Schneider, J.: A mirror furnace for neutron diffraction up to 2300 K. J. Appl. Crystallogr. **26** (1993) 632–635.

Megaw, H. D.: A note on the structure of lithium niobate, $LiNbO_3$. Acta Crystallogr. A**24** (1968a) 583–588.

Megaw, H. D.: The thermal expansion of interatomic bonds, illustrated by experimental evidence from certain niobates. Acta Crystallogr. A**24** (1968b) 589–604.

Megaw, H. D.: Crystal structures: A working approach. Philadelphia, Saunders, 1973.

Megaw, H. D.; Darlington, C. N. W.: Geometric and structural relations in thombohedral perovskites. Acta Crystallogr. A**31** (1975) 161–173.

Thomas, M. W.; Bendall, P. J.: A suite of programs for total profile refinement of number of powder diffraction patterns. Acta Crystallogr. A**34** (1978) 351.

Nakamura, K.; Ando, H.; Shimizu, H.: Ferroelectric domain inversion caused in $LiNbO_3$ plates by heat treatment. Appl. Phys. Lett. **48** (1987) 1413.

Zotov, N.; Frey, F.; Boysen, H.; Lehnert, H.; Hornsteiner, A.; Strauß, B.; Sonntag, R.; Mayer, M.; Güthoff, F.; Hohlwein, D.: X-ray and neutron diffuse scattering in $LiNbO_3$ from 38 to 1200 K. Acta Crystallogr. B**51** (1995) 961–972.